# Compatibilization of Immiscible Polymer Blends Using Graphene Oxide Sheets

**Yewen Cao, Jing Zhang, Jiachun Feng,* and Peiyi Wu**

Key Laboratory of Molecular Engineering of Polymers of Ministry of Education, Department of Macromolecular Science and Laboratory of Advanced Materials, Fudan University, Shanghai 200433, P.R. China

**ABSTRACT** By taking the advantage of the unique amphiphilic structure of graphene oxide sheets (GOSs), we develop here a new and effective strategy for compatibilizing immiscible polymer blends. With the incorporation of only 0.5 wt % GOSs into immiscible polyamide/polyphenylene oxide (PA/PPO, 90/10) blends, the droplet diameter of the dispersed minor phase (PPO) is dramatically reduced by more than 1 order of magnitude, indicating a largely improved compatibility in the GOS-filled polymer blends. As a result, the ductility of GOS-compatibilized polymer blends is notably elevated. The compatibilizing effect of GOSs should be due to the fact that GOSs can exhibit strong interactions with both PA and PPO phases, thus minimizing their interfacial tension. Moreover, unlike traditional copolymer compatibilizers, GOSs can also act as reinforcing fillers in polymer blends, thus remarkably enhancing their mechanical strength and thermal stability. Considering the inexpensive sources (graphite powders) and extraordinary properties of GOSs, this work may open up opportunities to produce new compatibilizers that are of great interest in the industrial field.

**KEYWORDS:** graphene oxide sheets · polymer blends · compatibilizers · reinforcing agents · mechanical properties · thermal stability

Over the past few decades, polymer blends have attracted considerable scientific and industrial interest because they play an important role in the modern polymer industry not only for the development of new materials but also for practical recycling. By varying the composition and the types of polymers that are mixed, the properties of polymer blends can be finely tuned. Unfortunately, because of the large unfavorable enthalpy of mixing, most polymer blends tend to macrophase separate, which leads to a deterioration in mechanical properties.[1] Therefore, controlling the phase behavior and morphology becomes a key factor in converting these immiscible blends into useful polymeric products. The traditional method to manipulate the interface properties of polymer blends is adding some copolymers (block, graft, or star) as compatibilizers.[2] In general, the added copolymers are compatible with both phases, thereby segregating preferentially at the interface and ensuring strong interfacial adhesion. A typical example of this strategy is the copolymer-compatibilized polyamide/polyphenylene oxide (PA/PPO) blend,[3−8] which has been developed as a commercial product. The copolymer-compatibilized PA/PPO blends can display greatly improved compatibility and thus achieve an excellent combination of the good melt processability and solvent resistance of PA with the high dimensional stability and water resistance of PPO. However, this conventional compatibilization route suffers from certain drawbacks. First, copolymers themselves have little benefit to the strength and stiffness of polymer blends because they tend to be "soft" materials. In some cases, their addition even weakens the mechanical properties.[3,9] Furthermore, copolymers with specific structure are often not easily synthesized, which makes them relatively expensive to engineer.[10] Therefore, searching for another potent compatibilization strategy at low cost is highly desirable.

Graphene oxide sheets (GOSs) are monolayers of $sp^2$-hybridized carbon atoms derivatized by a mixture of carboxyl, hydroxyl, and epoxy functionalities[11,12] and decorated with strongly bound oxidative debris.[13] They can be easily acquired from natural graphite flakes by strong oxidation and subsequent exfoliation. In the past few years, GOSs and their derivatives have been extensively studied in the context of many applications, such as polymer composites, biosensors, and drug delivery.[14] Especially, the extraordinary properties combined with the large aspect ratio and inexpensive sources of GOSs have spurred intensive interest in developing high-performance, cost-effective polymer composites.[15−17] It has been reported that the electrical, mechanical, thermal, and gas barrier properties of polymers can be remarkably improved by the incorporation of GOSs.[18−23] It should be noted that the

* Address correspondence to jcfeng@fudan.edu.cn.

Received for review May 10, 2011 and accepted June 15, 2011.

**Published online June 15, 2011**
**10.1021/nn201717a**

oxygen functional groups on GOSs also favor the utilization of these carbon nanostructures in polymer composites because they can enhance the interfacial interaction between GOS fillers and polymer matrices.[15] For example, Song and co-workers reported that GOSs could form strong hydrogen bonds with the amide groups of PA chains, and thus notably improve the mechanical properties of PA.[18]

Recently, there are some pioneering works devoted to the surface activity of GOSs.[24−27] According to Huang and co-workers, GOSs represent a unique type of building block with hydrophobic $\pi$ domains on the basal plane and hydrophilic carboxylic groups on the edges.[24] Therefore, GOSs exhibit an amphiphilic character and can be used as surfactants in numerous technological fields. For example, four independent groups have explored GOSs as dispersants to suspend otherwise insoluble carbon nanotubes in water.[24,28−30] Despite the substantial interest and effort in utilizing GOSs as dispersants, to the best of our knowledge, there is no work specifically dedicated to the usage of GOSs for compatibilizing immiscible polymer blends, which appears to be of more practical significance in that it can fully exploit the extraordinary properties of these appealing carbon nanomaterials.

In the present work, we reveal the potential of GOSs to be developed as potent and inexpensive compatibilizers by using them to compatibilize immiscible PA/PPO blends, blends that have been widely investigated as we mentioned above. With the addition of only 0.5 wt % GOSs, the PA/PPO (90/10) blends exhibit a significantly improved compatibility, as reflected by the dramatic decrease in the droplet size of the dispersed minor phase (PPO). The compatibilizing effect of GOSs should be due to the fact that GOSs can strongly interact with both PA and PPO phases, thus enhancing their interfacial adhesion. Moreover, the incorporation of GOSs also leads to considerable increases in mechanical strength and thermal stability in the resulting blends, indicating that GOSs are preferable to traditional copolymer compatibilizers and have a promising future in the industrial field.

## RESULTS AND DISCUSSION

GOSs are suggested to be amphiphilic substances with a largely hydrophobic basal plane and hydrophilic edges.[24] Therefore, they can exhibit strong interactions with both nonpolar polymers and polar polymers with potential use as compatibilizers for immiscible polymer blends. The addition of GOSs into polymer blends cannot only improve their compatibility but also enhance their mechanical and thermal performances, which makes GOSs preferable to traditional copolymer compatibilizers.

**Strong Interactions of GOSs with PPO and PA.** GOSs are reported to be able to adsorb nonpolar polymers on their basal planes through $\pi-\pi$ stackings or hydrophobic interactions.[31,32] The favorable interaction between GOSs and nonpolar PPO can be confirmed by the characterization of GOS−PPO hybrids, which were prepared through a noncovalent strategy. Figure 1 displays the FTIR spectra of PPO, GOSs, and PPO−GOS hybrids. Compared with the FTIR spectrum of GOSs, that of GOS−PPO hybrids presents two distinct bands at 2920 and 2854 $cm^{-1}$, which correspond to the asymmetric C−H stretch of methyl groups in PPO. It should be noted that the GOS−PPO hybrids underwent a harsh rinsing process until no trace of PPO was detected in the filtrate, suggesting that the remaining PPO is tightly adsorbed onto GOS basal planes and cannot be washed away. The TG and derivative TG (DTG) curves of GOS−PPO hybrids are illustrated in Figure 2. Two major weight loss peaks can be found in the DTG plot. The first one, which appears at 213 °C, should be attributed to the pyrolysis of the oxide functional groups.[33] The second peak at approximately 441 °C corresponds to the decomposition of PPO (Supporting Information, Figure S1). The weight loss due to polymer decomposition is about 17%, indicating that 1 mg of GOSs can adsorb around 0.2 mg of PPO on their basal planes.

In general, the immobilization of polymers on GOSs would affect their thickness and morphology. Therefore, AFM was taken to observe the GOS−PPO hybrids. As depicted in Figure 3, the measured thickness of

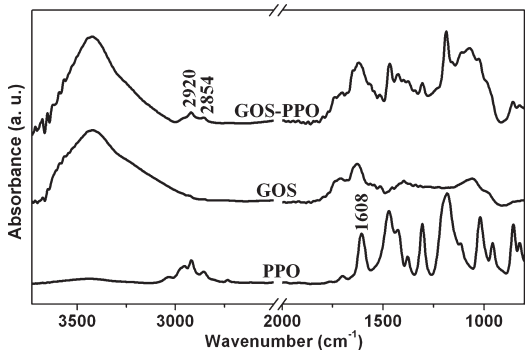


Figure 1. FTIR spectra of PPO, GOSs, and PPO−GOS hybrids.

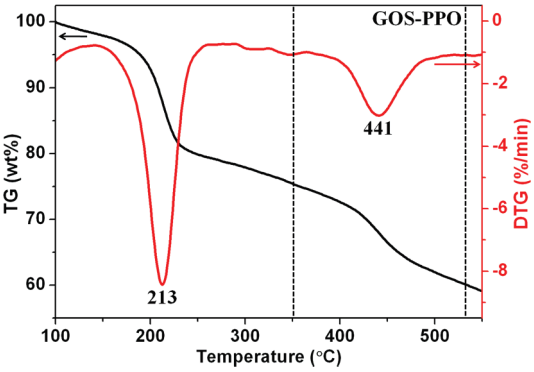


Figure 2. TG and DTG curves for GOS−PPO hybrids.

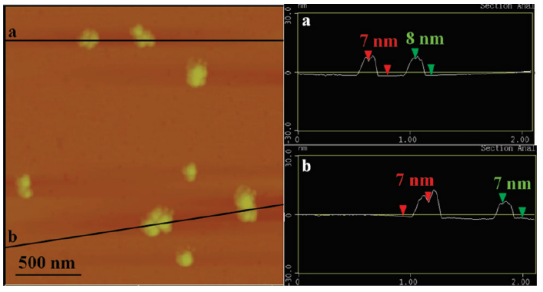


**Figure 3. AFM image (left) and height profiles (right) of GOS–PPO hybrids.**

GOS–PPO hybrids is very uniform (7–8 nm), and no platelet with one-half or one-third of this thickness was detected, indicating that the observed sheets are uniform monolayers. It should be noted that the GOS–PPO hybrids are much thicker than GOSs, whose height is about 1.4 nm (Supporting Information, Figure S2 matching well with the reported thickness of individual GOSs).[34] Similar thickness increases have also been reported for polymer-coated GOSs.[31,32,35,36] For example, Xu *et al*. found that the *in situ* polymerization of caprolactam on GOSs would increase their height to 8 nm.[35] Moreover, in contrast to the smooth surfaces of GOSs (Supporting Information, Figure S2), the surfaces of GOS–PPO hybrids are rather coarse (Figure 3), which is mainly generated from the polymer wrapping and folding. The similar phenomenon has also been reported by Liu and co-workers, who noncovalently functionalized GOSs with polyacrylamide.[36] The transformations of the thickness and morphology of sheets verify the tight attachment of PPO onto GOS surfaces.

It has been widely reported that the hydrophilic groups at the GOS edges can form strong hydrogen bonding with polar polymers, such as poly(vinyl alcohol),[19] poly(methyl methacrylate),[20] and polyurethane.[21] As a typical polar polymer, PA should also be able to strongly interact with the hydrophilic edges of GOSs through hydrogen bonding. To corroborate it, the FTIR investigations were conducted on PA/PPO blends with and without GOS addition. As we can see in Figure 4a, there are several absorptions in the FTIR spectrum of uncompatibilized PA/PPO blend. The doublet at 2920 and 2850 $cm^{-1}$ corresponds to the asymmetric C–H stretching of methyl and methylene groups in PA, while the peak at 3295 $cm^{-1}$ is ascribed to the asymmetric N–H stretching of amide groups in PA. Upon the introduction of GOSs, the band belonging to the N–H stretching shifts down to 3291 $cm^{-1}$ (Figure 4b), while those assigned to C–H stretching do not present any change (Supporting Information, Figure S3). Such a blue shift of the peak of N–H stretching has also been reported in GOS-reinforced PA composites and was attributed to the formation of hydrogen bonding between the oxygen functionalities at GOS edges and the amide groups in PA.[18] As a result, the intimate interaction of GOSs with PA is well addressed.

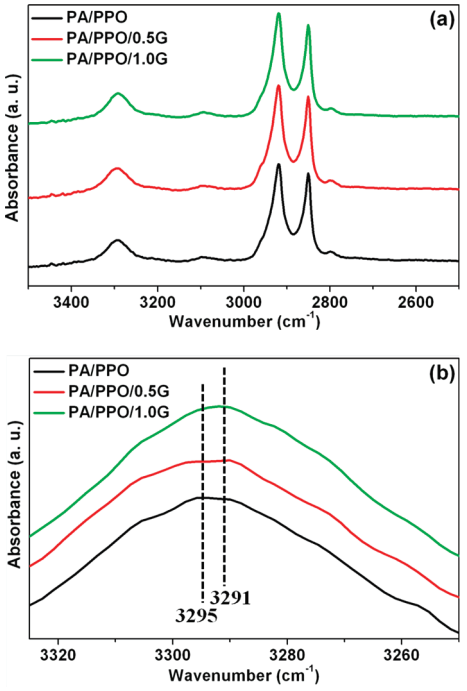


**Figure 4. (a) FTIR spectra and (b) their enlarged image for the N–H stretching peak of uncompatibilized and GOS-compatibilized PA/PPO blends.**

**Compatibilizing Effect of GOSs in Polymer Blends.** Considering the strong interactions of GOSs with PPO and PA as we confirmed above, the addition of GOSs into PA/PPO blends should be able to minimize their interfacial tension, thus leading to a notably improved compatibility. The compatibilizing effect of GOSs in PA/PPO blends is demonstrated by SEM micrographs, which are shown in Figures 5 and 6. To identify the minor PPO phase, the specimens for SEM observations were immersed in THF with the aid of sonication for 4 h so that the dispersed PPO can be removed. Consequently, in the SEM images, the PPO phase appears as holes in the matrix of the major PA phase. In the uncompatibilized PA/PPO blend, these PPO holes are quite large with a diameter of more than 10 $\mu$m (Figure 5a). These holes can be easily detected even at a magnification of $\times$500 (Supporting Information, Figure S4a). With the addition of 0.5 or 1.0 wt % GOSs, a dramatic decrease in the size of the PPO domains occurs as these huge holes convert into tiny pores that are not visible at a magnification of $\times$500 (Supporting Information, Figure S4b,c). Increasing the magnification to $\times$2000 reveals the presence of these small pores as one can meticulously perceive in Figure 5b,c. By further raising the magnification to $\times$5000, we can find that the droplet diameter of the PPO phase in GOS-compatibilized polymer blends is less than 1 $\mu$m (Figure 6), which is more than 1 order of magnitude lower than that in uncompatibilized PA/PPO blend. In polymer blends, the better is the compatibility, the more uniform is the dispersion of one phase in another.[2] Therefore, we can conclude that the

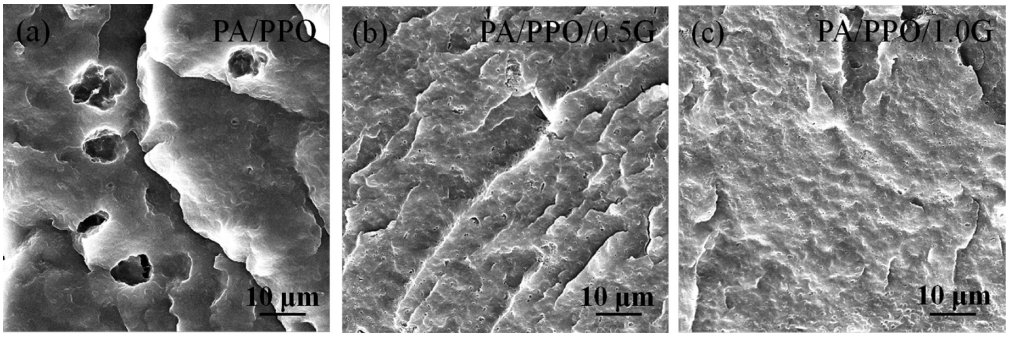


**Figure 5. SEM micrographs for the cryogenically fractured surfaces of uncompatibilized and GOS-compatibilized PA/PPO blends after THF etching at a magnification of ×2000.**

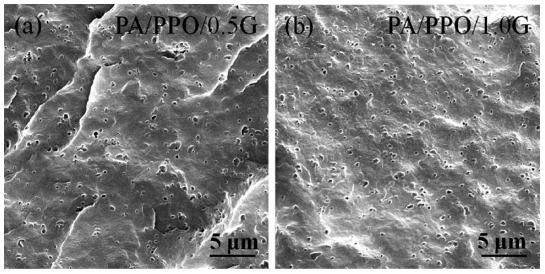


**Figure 6. SEM micrographs for the cryogenically fractured surfaces of (a) PA/PPO/0.5G and (b) PA/PPO/1.0G blends after THF etching at a magnification of ×5000.**

compatibilizing efficiency of GOSs in PA/PPO blends is quite prominent even at very low GOS concentration (*e.g.*, 0.5 wt %). Moreover, it is also observed from Figure 6 that compared to that in PA/PPO/0.5G, the droplet of the dispersed PPO domains in PA/PPO/1.0G becomes finer and more uniform, indicating that the compatibilizing effect of GOSs is also related to their loading.

Figure 7 displays the schematic description of the compatibilizing mechanism of GOSs in the PA/PPO blends. For uncompatibilized PA/PPO blend, macrophase separation prevails because of the high interfacial tension between PA and PPO. With the addition of GOSs, these sheets can adsorb PPO on their basal planes while form strong hydrogen bonding with PA through their edge-located oxygen functional groups. Therefore, they migrate to the interface and weave across the interface, allowing the formation of entanglements and reducing unfavorable contacts. As a result, GOSs can minimize the interfacial tension and improve the compatibility of PA/PPO blends.

In terms of the commercial applicability, melt processing is the most economically attractive method for producing polymer blends because it is scalable, versatile, and environmentally friendly.[37] Therefore, a parallel sample, which is denoted as *m*-PA/PPO/1.0G, was fabricated by a direct melt blending of PA, PPO, and GOSs. In the *m*-PA/PPO/1.0G blend, the droplet size of the PPO domains is about 10 $\mu$m, as reflected by SEM images (Supporting Information, Figure S5). This value is almost the same as that in the uncompatibilized PA/PPO blend, indicating that the compatibilizing effect of GOSs is nearly absent in the *m*-PA/PPO/1.0G blend. It may be due to the insufficient contact of PPO and GOSs during the melt compounding process. Generally, the $\pi-\pi$ stacking interactions are realized by a solvent mixing of two components for a long time,[32] because it allows a full contact of these two components. For example, in this study, PPO/GOS master batch was prepared by blending PPO with GOSs in THF for 3 h.

**Performances of GOS-Compatibilized Polymer Blends.** Unlike traditional copolymer compatibilizers, which tend to be "soft" materials, GOSs are mechanically rigid with an effective Young's modulus of more than 200 GPa,[38] and have been widely used as reinforcing fillers for high-performance composites.[15] Therefore, the incorporation of GOSs into PA/PPO blends should not only improve their compatibility, but also enhance their mechanical and thermal properties. The representative stress−strain curves of uncompatibilized and GOS-compatibilized PA/PPO blends are given in Figure 8a. Compared to uncompatibilized PA/PPO blend, GOS-compatibilized PA/PPO blends exhibit largely increased elongations with observed yield behavior. The remarkably enhanced ductility after GOS addition should be assigned to the prominent compatibilizing effect of GOSs, as we have illustrated above. Moreover, the introduction of GOSs can also notably increase the mechanical strength of polymer blends, which may be due to the ultrahigh strength of GOSs as well as the substantially improved dispersion of PPO, as we will discuss below. Figure 8b demonstrates the elongation and tensile strength data of all the samples. It is obvious that these two parameters have a pronounced increasing tendency with increase of GOS loading. With only 1.0 wt % GOSs filled, the elongation increases by 89% from 28.6% (for uncompatibilized PA/PPO blend) to 54.0%, while the tensile strength is raised by 87% from 17.5 MPa (for uncompatibilized PA/PPO blend) to 32.7 MPa.

It may be interesting to compare the mechanical properties of GOS- and copolymer-compatibilized PA/PPO

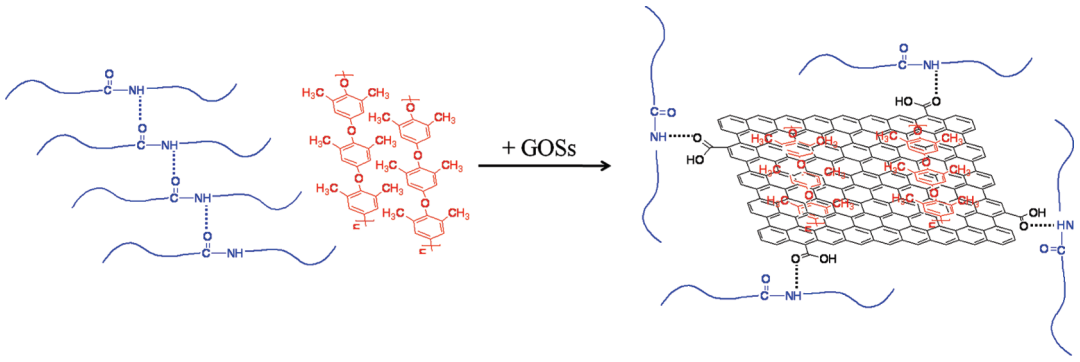


Figure 7. Schematic description of the compatibilizing mechanism of GOSs in the PA/PPO blends.

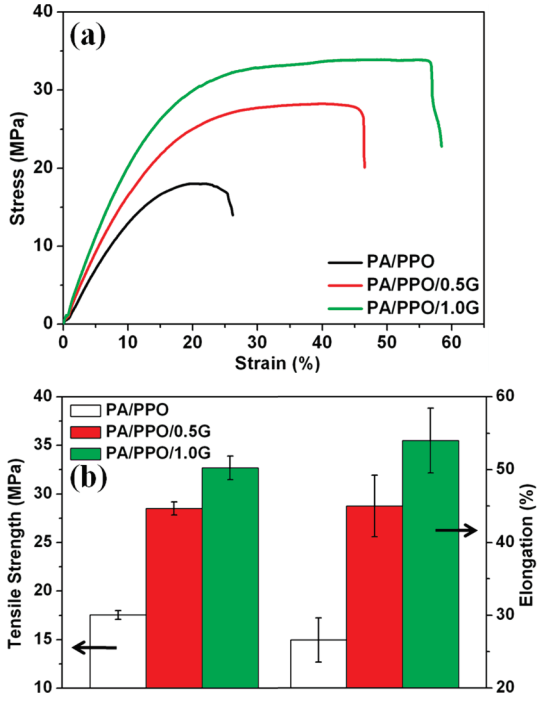


Figure 8. (a) Representative stress–strain curves as well as (b) tensile strength and elongation data of uncompatibilized and GOS-compatibilized PA/PPO blends.

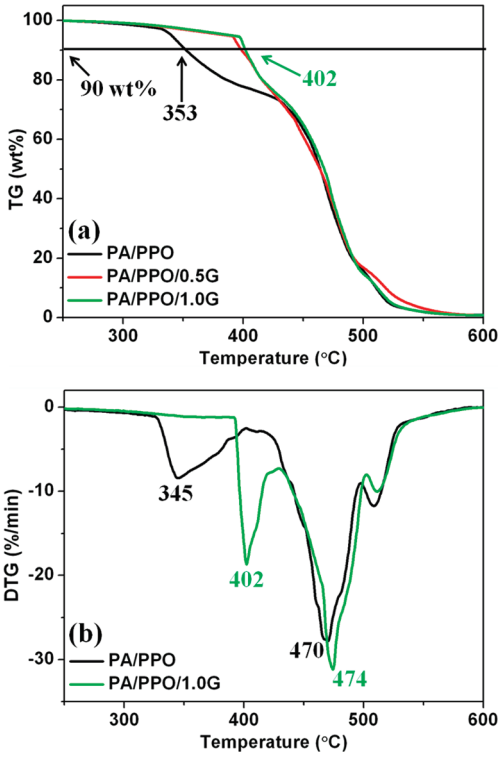


Figure 9. (a) TG and (b) DTG traces for uncompatibilized and GOS-compatibilized PA/PPO blends.

blends. In a previous study, Li *et al.* used three kinds of copolymers to compatibilize PA/PPO blends. In all the cases, the compatibility of the blends was improved, while the tensile strength decreased with increasing copolymer content.[3] Such results are to be expected because copolymers tend to be "soft" materials, and thus their introduction is not beneficial to mechanical reinforcement. In GOS-compatibilized PA/PPO blends, GOSs can serve as not only compatibilizers but also reinforcing agents because of their extraordinary mechanical properties. As a result, the tensile strength of GOS-compatibilized PA/PPO blends is substantially increased, suggesting that GOSs are preferable to traditional copolymer compatibilizers. It should be noted that such an outstanding mechanical reinforcement (87% increase in tensile strength) may not be ascribed to the ultrahigh strength of GOSs only. According to Leibler and co-workers, the greatly improved compatibility of polymer blends can result in notable increases in their mechanical strength, even when the minor phase is just a small portion.[39] Therefore, the remarkably enhanced dispersion of high-strength PPO[7] in the PA should also play an important role in the prominent mechanical reinforcement. To clarify it, PA and PA/1.0G composite were fabricated to evaluate the basic reinforcement of GOSs to neat PA matrix. As shown in Supporting Information, Figure S6, the yield strength of PA/1.0G composite is only 22% higher than that of PA, suggesting that the reinforcing effect of GOSs on neat PA matrix is limited when compared to that on PA/PPO matrix. Consequently, we can conclude that the prominent mechanical reinforcement in the PA/PPO/1.0G blend is due to both

the reinforcing effect of GOSs and the enhanced dispersion of PPO.

The effect of GOS addition on the thermal stability of polymer blends was also investigated. Figure 9a displays the TG traces of uncompatibilized and GOS-compatibilized PA/PPO blends. Obviously, the incorporation of GOSs induces thermal stabilization of the matrix: the temperature for 10% weight loss increases by around 50 °C from 353 (for uncompatibilized PA/PPO blend) to 402 °C (for PA/PPO/1.0G blend). Such an enhancement in thermal stability is to be expected because GOSs are proposed to act as barriers in polymer matrices to delay the permeation of oxygen and the escape of volatile degradation products, thus improving the thermal stability of the resulting polymer blends.[15] The DTG plots of uncompatibilized PA/PPO and PA/PPO/1.0G blends are shown in Figure 9b. It can be observed that the uncompatibilized PA/PPO blend exhibits a two-stage decomposition process; a minor mass loss peak at 345 °C followed by a major one at 470 °C. The introduction of GOSs stabilizes the matrix against the first stage of decomposition while having little influence on the second stage of decomposition. Similar results have also been reported in carbon nanofiber-reinforced PA composites and were ascribed to the radical capture by carbon nanofillers.[40]

## CONCLUSIONS

We have revealed the potential of GOSs to be developed as potent compatibilizers by using them to compatibilize immiscible PA/PPO blends. With the addition of only 0.5 wt % GOSs, the droplet diameter of the dispersed minor phase (PPO) is dramatically reduced by more than 1 order of magnitude, indicating that the compatibilizing efficiency of GOSs is rather prominent even at low content. The compatibilizing effect of GOSs should be due to the fact that they can adsorb PPO on their basal planes while forming strong hydrogen bonds with PA through their edge-located oxygen functional groups, thus acting as coupling agents for the two components. In addition, as ideal reinforcing fillers, GOSs can also remarkably enhance the mechanical and thermal performances of PA/PPO blends. With the incorporation of 1.0 wt % GOSs, the tensile strength increases by 87%, while the temperature for 10% weight loss is raised by about 50 °C. Considering the inexpensive sources (graphite powders) and extraordinary properties of GOSs, this work may open up opportunities to produce new compatibilizers that are of great interest in the industrial field.

## MATERIALS AND METHODS

**Materials.** Graphite oxide powders were synthesized from expandable graphite powders (Yingtai Company, China) using a modified Hummers method.[41] PA used in this study is PA12 (Grilamid L25W20X, EMS-Chemie, Switzerland) with a melt flow rate of 20 g/10 min (275 °C, 5.0 kg). Prior to melt processing, PA12 pellets were dried in an oven at 80 °C for 24 h to remove residual moisture. PPO with an intrinsic viscosity of $0.57 \times 10^{-3}$ $m^3/kg$ in chloroform was provided by Institute of Chemical Engineering of Beijing, China. Unless otherwise stated, all other reagents and solvents were purchased from commercial suppliers and used as received.

**Preparation of GOS–PPO Hybrids.** To corroborate the favorable interaction between GOSs and PPO, their hybrids were prepared through a noncovalent approach. Typically, 5 mg of graphite oxide powders was suspended in 20 mL of tetrahydrofuran (THF) and exfoliated into single-layer GOSs with the aid of sonication.[34] Then, the GOS dispersion was mixed with a THF solution of 50 mg of PPO and stirred overnight. Obtained from the mixture by vacuum filtration, the solids were redispersed in 150 mL of THF and separated by vacuum filtration again. This purification cycle was repeated four times, and the final products were dried at 35 °C under vacuum overnight, yielding GOS–PPO hybrids. In the last cycle, the filtrate was carefully collected for a FTIR measurement. The FTIR spectrum of the filtrate is almost the same as that of pure THF, and the absorption at 1608 $cm^{-1}$ for the C=C stretch of PPO cannot be observed (Supporting Information, Figure S7), indicating that the filtrate is free of PPO.

**Characterization of GOSs and GOS–PPO Hybrids.** FTIR spectra were recorded on a Shimadz IRPrestige-21 spectrophotometer using KBr pellets. AFM graphs were acquired with a Multimode Nano 4 in the tapping mode. Thermogravimetric analysis (TGA) was carried out under nitrogen atmosphere with a Netzsch TG 209F1 at a heating rate of 20 °C/min.

**Fabrication of GOS-Compatibilized Polymer Blends.** The GOS-compatibilized PA/PPO blends were fabricated *via* a two-step procedure: Solvent blending of PPO and GOSs, and subsequent melt compounding of PA and the PPO/GOS master batch. In the solvent blending step, 200 (400) mg of GOSs were dispersed in 80 mL of THF with the aid of sonication. Afterward, 3.8 (3.6) g of PPO was added to the suspension. After agitation at 50 °C for 2 h and sonication at 45 °C for another 1 h, the mixture was coagulated with 800 mL of methanol. The flocculent was filtered under vacuum, and then vacuum-dried at 40 °C for 12 h, yielding a PPO/5 wt % GOS (PPO/10 wt % GOS) master batch. In the latter stage, each of the above master batches was added into 36 g of PA, and melt mixed at 210 °C for 10 min with a screw speed of 60 rpm using a Haake-Rheomix. As a result, blends of PA/PPO/GOS (90/9.5/0.5) and PA/PPO/GOS (90/9.0/1.0), which are denoted as PA/PPO/0.5G and PA/PPO/1.0G, respectively, were obtained. For comparison, uncompatibilized PA/PPO (90/10) was fabricated in the same manner. In addition, a parallel sample was fabricated by a direct melt blending of 36 g of PA, 3.6 g of PPO, and 0.4 g of GOSs. For convenience, this sample is denoted as *m*-PA/PPO/1.0G. PA, and PA/1.0G (PA composite with 1 wt % GOSs) was also produced through a melt process. These samples were compression molded (210 °C, 5 MPa) into 0.4–0.45 mm thick sheets or injection molded (220 °C) into dog-bone type specimens for the following measurement. The dimensions of the dog-bone type specimens are 40 mm (length) × 15 mm (width) × 20 mm (narrow portion length) × 4.5 mm (narrow portion width) × 1.0 mm (thickness). Note that the samples were dried in an oven at 80 °C for 24 h before compression and injection molding.

**Measurement of GOS-Compatibilized Polymer Blends.** FTIR examinations were conducted on a Nicolet Nexus 470 spectrometer equipped with an OMNI-Sampler. Thermal stability was estimated by TGA assays (Perkin-Elmer, heating from 50 to 650 °C at a rate of 20 °C/min in air). To investigate the compatibilizing

effect of GOSs in polymer blends, the cryogenically fractured surfaces of the dog-bone type specimens were observed with scanning electron microscopy (SEM, TESCAN 5136MM). Before SEM observations, the cryogenically fractured surfaces were etched in THF with the assistance of sonication for 4 h to remove the PPO phase, and then Aurum sputter coated. Mechanical properties were evaluated at 23 °C and ~25% relative humidity using a universal testing machine (CMT-4102, SANS Group, China) with a crosshead speed of 5 mm/min for the dog-bone type specimens. At least five tests were performed for each sample, from which the mean values and standard deviations were derived.

*Acknowledgment.* This work was financially supported by National Science Foundation of China (20874017), Shanghai-Unilever Research & Development Fund (09520715500), and National Basic Research Program of China(2011CB605700).

*Supporting Information Available:* Additional FTIR spectra and SEM graphs, TG and DTG traces for PPO, AFM image of GOSs, and mechanical data of PA and PA/1.0G. This material is available free of charge *via* the Internet at http://pubs.acs.org.

## REFERENCES AND NOTES


1. Utracki, L. A. *Polymer Alloys and Blends*; Hanser Publishers: New York, 1990.
2. Paul, D. R.; Bucknall, C. B. *Polymer Blends: Formulation and Performance*; John Wiley & Sons: New York, 2000.
3. Li, B.; Wan, C. Y.; Zhang, Y.; Ji, J. L. Blends of Poly(2,6-dimethyl-1,4-phenylene oxide)/Polyamide 6 Toughened by Maleated Polystyrene-Based Copolymers: Mechanical Properties, Morphology, and Rheology. *J. Appl. Polym. Sci.* **2010**, *115*, 3385–3392.
4. Campbell, J. R.; Hobbs, S. Y.; Shea, T. J.; Watkins, V. H. Poly(Phenylene Oxide) Polyamide Blends *via* Reactive Extrusion. *Polym. Eng. Sci.* **1990**, *30*, 1056–1062.
5. Chiang, C. R.; Chang, F. C. Polymer Blends of Polyamide-6 (PA6) and Poly(Phenylene Oxide) (PPO) Compatibilized by Styrene-Maleic Anhydride (SMA) Copolymer. *Polymer* **1997**, *38*, 4807–4817.
6. Tjong, S. C.; Ke, Y. C. Fracture Toughening Behavior of Elastomer Modified Polyphenylene Ether Polyamide Blends. *Eur. Polym. J.* **1998**, *34*, 1565–1570.
7. Wang, X. D.; Feng, W.; Li, H. Q.; Jin, R. G. Compatibilization and Toughening of Poly(2,6-dimethyl-1,4-phenylene oxide)/Polyamide 6 Alloy with Poly(ethylene 1-octene): Mechanical Properties, Morphology, and Rheology. *J. Appl. Polym. Sci.* **2003**, *88*, 3110–3116.
8. Wu, D. Z.; Wang, X. D.; Jin, R. G. Toughening of Poly(2,6-dimethyl-1,4-phenylene oxide)/Nylon 6 Alloys with Functionalized Elastomers *via* Reactive Compatibilization: Morphology, Mechanical Properties, and Rheology. *Eur. Polym. J.* **2004**, *40*, 1223–1232.
9. Barhoumi, N.; Jaziri, M.; Massardier, V.; Cassagnau, P. Valorization of Poly(butylene terephthalate) Wastes by Blending with Virgin Polypropylene: Effect of the Composition and the Compatibilization. *Polym. Eng. Sci.* **2008**, *48*, 1592–1599.
10. Si, M.; Araki, T.; Ade, H.; Kilcoyne, A. L. D.; Fisher, R.; Sokolov, J. C.; Rafailovich, M. H. Compatibilizing Bulk Polymer Blends by Using Organoclays. *Macromolecules* **2006**, *39*, 4793–4801.
11. Lerf, A.; He, H. Y.; Forster, M.; Klinowski, J. Structure of Graphite Oxide Revisited. *J. Phys. Chem. B* **1998**, *102*, 4477–4482.
12. Wilson, N. R.; Pandey, P. A.; Beanland, R.; Young, R. J.; Kinloch, I. A.; Gong, L.; Liu, Z.; Suenaga, K.; Rourke, J. P.; York, S. J.; *et al*. Graphene Oxide: Structural Analysis and Application as a Highly Transparent Support for Electron Microscopy. *ACS Nano* **2009**, *3*, 2547–2556.
13. Rourke, J. P.; Pandey, P. A.; Moore, J. J.; Bates, M.; Kinloch, I. A.; Young, R. J.; Wilson, N. R. The Real Graphene Oxide Revealed: Stripping the Oxidative Debris from the Graphene-like Sheets. *Angew. Chem., Int. Ed.* **2011**, *50*, 3173–3177.
14. Dreyer, D. R.; Park, S.; Bielawski, C. W.; Ruoff, R. S. The Chemistry of Graphene Oxide. *Chem. Soc. Rev.* **2010**, *39*, 228–240.
15. Cai, D. Y.; Song, M. Recent Advance in Functionalized Graphene/Polymer Nanocomposites. *J. Mater. Chem.* **2010**, *20*, 7906–7915.
16. Kim, H.; Abdala, A. A.; Macosko, C. W. Graphene/Polymer Nanocomposites. *Macromolecules* **2010**, *43*, 6515–6530.
17. Potts, J. R.; Dreyer, D. R.; Bielawski, C. W.; Ruoff, R. S. Graphene-Based Polymer Nanocomposites. *Polymer* **2011**, *52*, 5–25.
18. Rafiq, R.; Cai, D. Y.; Jin, J.; Song, M. Increasing the Toughness of Nylon 12 by the Incorporation of Functionalized Graphene. *Carbon* **2010**, *48*, 4309–4314.
19. Liang, J. J.; Huang, Y.; Zhang, L.; Wang, Y.; Ma, Y. F.; Guo, T. Y.; Chen, Y. S. Molecular-Level Dispersion of Graphene into Poly(vinyl alcohol) and Effective Reinforcement of their Nanocomposites. *Adv. Funct. Mater.* **2009**, *19*, 2297–2302.
20. Ramanathan, T.; Abdala, A. A.; Stankovich, S.; Dikin, D. A.; Herrera-Alonso, M.; Piner, R. D.; Adamson, D. H.; Schniepp, H. C.; Chen, X.; Ruoff, R. S.; *et al*. Functionalized Graphene Sheets for Polymer Nanocomposites. *Nat. Nanotechnol.* **2008**, *3*, 327–331.
21. Kim, H.; Miura, Y.; Macosko, C. W. Graphene/Polyurethane Nanocomposites for Improved Gas Barrier and Electrical Conductivity. *Chem. Mater.* **2010**, *22*, 3441–3450.
22. Rafiee, M. A.; Rafiee, J.; Wang, Z.; Song, H. H.; Yu, Z. Z.; Koratkar, N. Enhanced Mechanical Properties of Nanocomposites at Low Graphene Content. *ACS Nano* **2009**, *3*, 3884–3890.
23. Wu, J. H.; Tang, Q. W.; Sun, H.; Lin, J. M.; Ao, H. Y.; Huang, M. L.; Huang, Y. F. Conducting Film from Graphite Oxide Nanoplatelets and Poly(acrylic acid) by Layer-by-Layer Self-Assembly. *Langmuir* **2008**, *24*, 4800–4805.
24. Kim, J.; Cote, L. J.; Kim, F.; Yuan, W.; Shull, K. R.; Huang, J. X. Graphene Oxide Sheets at Interfaces. *J. Am. Chem. Soc.* **2010**, *132*, 8180–8186.
25. Luo, J. Y.; Cote, L. J.; Tung, V. C.; Tan, A. T. L.; Goins, P. E.; Wu, J. S.; Huang, J. X. Graphene Oxide Nanocolloids. *J. Am. Chem. Soc.* **2010**, *132*, 17667–17669.
26. Kim, F.; Cote, L. J.; Huang, J. X. Graphene Oxide: Surface Activity and Two-Dimensional Assembly. *Adv. Mater.* **2010**, *22*, 1954–1958.
27. Tian, L. L.; Anilkumar, P.; Cao, L.; Kong, C. Y.; Meziani, M. J.; Qian, H. J.; Veca, L. M.; Thorne, T. J.; Tackett, K. N.; Edwards, T.; *et al*. Graphene Oxides Dispersing and Hosting Graphene Sheets for Unique Nanocomposite Materials. *ACS Nano* **2011**, *5*, 3052–3058.
28. Qiu, L.; Yang, X. W.; Gou, X. L.; Yang, W. R.; Ma, Z. F.; Wallace, G. G.; Li, D. Dispersing Carbon Nanotubes with Graphene Oxide in Water and Synergistic Effects between Graphene Derivatives. *Chem.—Eur. J.* **2010**, *16*, 10653–10658.
29. Zhang, C.; Ren, L. L.; Wang, X. Y.; Liu, T. X. Graphene Oxide-Assisted Dispersion of Pristine Multiwalled Carbon Nanotubes in Aqueous Media. *J. Phys. Chem. C* **2010**, *114*, 11435–11440.
30. Tian, L. L.; Meziani, M. J.; Lu, F. S.; Kong, C. Y.; Cao, L.; Thorne, T. J.; Sun, Y. P. Graphene Oxides for Homogeneous Dispersion of Carbon Nanotubes. *ACS Appl. Mater. Interface.* **2010**, *2*, 3217–3222.
31. Zu, S. Z.; Han, B. H. Aqueous Dispersion of Graphene Sheets Stabilized by Pluronic Copolymers: Formation of Supramolecular Hydrogel. *J. Phys. Chem. C* **2009**, *113*, 13651–13657.
32. Bai, H.; Xu, Y. X.; Zhao, L.; Li, C.; Shi, G. Q. Non-covalent Functionalization of Graphene Sheets by Sulfonated Polyaniline. *Chem. Commun.* **2009**, 1667–1669.
33. Cao, Y. W.; Yang, T.; Feng, J. C.; Wu, P. Y. Decoration of Graphene Oxide Sheets with Luminescent Rare-Earth Complexes. *Carbon* **2011**, *49*, 1502–1504.
34. Paredes, J. I.; Villar-Rodil, S.; Martinez-Alonso, A.; Tascon, J. M. D. Graphene Oxide Dispersions in Organic Solvents. *Langmuir* **2008**, *24*, 10560–10564.
35. Xu, Z.; Gao, C. *In situ* Polymerization Approach to Graphene-Reinforced Nylon-6 Composites. *Macromolecules* **2010**, *43*, 6716–6723.
36. Ren, L. L.; Liu, T. X.; Guo, J. A.; Guo, S. Z.; Wang, X. Y.; Wang, W. Z. A Smart pH Responsive Graphene/Polyacrylamide Complex *via* Noncovalent Interaction. *Nanotechnology* **2010**, *21*, 335701.

37. Verdejo, R.; Bernal, M. M.; Romasanta, L. J.; Lopez-Manchado, M. A. Graphene Filled Polymer Nanocomposites. *J. Mater. Chem.* **2011**, *21*, 3301–3310.
38. Suk, J. W.; Piner, R. D.; An, J.; Ruoff, R. S. Mechanical Properties of Monolayer Graphene Oxide. *ACS Nano* **2010**, *4*, 6557–6564.
39. Pernot, H.; Baumert, M.; Court, F.; Leibler, L. Design and Properties of Co-Continuous Nanostructured Polymers by Reactive Blending. *Nat. Mater.* **2002**, *1*, 54–58.
40. Sandler, J. K. W.; Pegel, S.; Cadek, M.; Gojny, F.; van Es, M.; Lohmar, J.; Blau, W. J.; Schulte, K.; Windle, A. H.; Shaffer, M. S. P. A Comparative Study of Melt Spun Polyamide-12 Fibres Reinforced with Carbon Nanotubes and Nanofibres. *Polymer* **2004**, *45*, 2001–2015.
41. Cao, Y. W.; Feng, J. C.; Wu, P. Y. Preparation of Organically Dispersible Graphene Nanosheet Powders through a Lyophilization Method and Their Poly(lactic acid) Composites. *Carbon* **2010**, *48*, 3834–3839.